

## *In situ* X-Ray Diffraction of Shock-Compressed Fused Silica

Sally June Tracy,<sup>1,\*</sup> Stefan J. Turneure,<sup>2</sup> and Thomas S. Duffy<sup>1</sup><sup>1</sup>*Department of Geosciences, Princeton University, Princeton, New Jersey 08544, USA*<sup>2</sup>*Institute for Shock Physics, Washington State University, Pullman, Washington 99164-2816, USA*

(Received 9 January 2018; published 29 March 2018)

Because of its widespread applications in materials science and geophysics, SiO<sub>2</sub> has been extensively examined under shock compression. Both quartz and fused silica transform through a so-called “mixed-phase region” to a dense, low compressibility high-pressure phase. For decades, the nature of this phase has been a subject of debate. Proposed structures include crystalline stishovite, another high-pressure crystalline phase, or a dense amorphous phase. Here we use plate-impact experiments and pulsed synchrotron x-ray diffraction to examine the structure of fused silica shock compressed to 63 GPa. In contrast to recent laser-driven compression experiments, we find that fused silica adopts a dense amorphous structure at 34 GPa and below. When compressed above 34 GPa, fused silica transforms to untextured polycrystalline stishovite. Our results can explain previously ambiguous features of the shock-compression behavior of fused silica and are consistent with recent molecular dynamics simulations. Stishovite grain sizes are estimated to be ~5–30 nm for compression over a few hundred nanosecond time scale.

DOI: 10.1103/PhysRevLett.120.135702

Laboratory shock wave experiments have long played an important role in the study of materials in extreme environments. Shock compression experiments provide the unique capability to study impact phenomena in real time and allow for measurements of equations of state [1–3], phase transitions [4,5], melting [6–9], sound velocities [5,10,11], the Grüneisen parameter [12,13], and transport properties [14]. However, a limitation of shock wave studies is that the *in situ* crystal structure of high-pressure phases formed under dynamic compression is generally not known.

Because of its fundamental importance in condensed matter physics and geophysics, SiO<sub>2</sub> is one of the most intensely studied materials under high-pressure conditions. Fused silica is widely used as an optical material, and its dynamic response is needed to understand high-powered laser-matter interactions and ballistic penetration [15–18]. SiO<sub>2</sub> is used as a model system for understanding the physics of amorphous materials at high pressures [19]. In addition, SiO<sub>2</sub> is the most abundant oxide constituent of Earth's crust and serves as an archetype for silicate crystals and melts of the deep Earth. As a result, the behavior of silica under dynamic loading is essential for modeling the effects of impacts and explosions in the crust. Despite its wide application, existing models of the dynamic response of SiO<sub>2</sub> [20–23] suffer from limitations arising from uncertainties about the structure of the high-pressure phase(s).

Based on pressure-density Hugoniot measurements, the shock-compression behavior of fused silica can be divided into three regions: (1) an elastic regime extending to 8–9 GPa, (2) a highly compressible region from 10 to 35 known as the

“mixed-phase region,” and (3) a dense, low compressibility phase above 35 GPa. Despite decades of study, the nature of the crystal structure or structures existing in the mixed- and high-pressure regions are not known. It is often assumed that the high-pressure phase corresponds to crystalline stishovite (or its CaCl<sub>2</sub>-type modification) as observed in static compression experiments and that the mixed-phase regime is a mixture of the low- and high-pressure forms [2,23,24] but direct proof is lacking. Luo *et al.* [20] have argued that shocked quartz transforms to stishovite (or a stishovitelike) phase between 15 and 46 GPa. Recent laser-driven compression experiments have suggested that stishovite may begin forming as low as 5 GPa [25]. Others have suggested that the high-pressure phase of SiO<sub>2</sub> corresponds to another high-pressure crystal structure [26,27] or an amorphous phase [21,28–33]. Recovery experiments generally find amorphous material with only trace quantities of stishovite [31,34], but due to the high-temperature release path, it is an open question whether amorphization occurs during compression or release. The formation of stishovite requires transformation of an initially tetrahedrally coordinated glass to a dense, octahedrally coordinated crystalline structure at high pressures. It has been argued that this would require a reconstructive phase transformation that would be too sluggish to occur on shock wave time scales [30].

To probe the crystal structure of fused silica under shock compression, we carried out time-resolved x-ray diffraction measurements coupled with gun-based dynamic compression. Plate impact loading provides uniform, well-defined conditions within the sample. The diffraction data are combined with continuum-level measurements to reveal a complete picture of the material response from the

atomic length scale to the continuum level, allowing for the unambiguous determination of the phase(s) formed at  $\sim 100$ -ns time scales from 12 to 63 GPa.

Plate impact experiments were carried out at the Dynamic Compression Sector of the Advanced Photon Source (APS). Planar shock waves in fused silica were generated using LiF impactors accelerated in a polycarbonate projectile to a velocity of 1.8–5.6 km/s using either a single-stage propellant gun or a two-stage light gas gun. A schematic of the impact configuration is shown in the Supplemental Material Fig. S4 [35]. The resulting stress states in the sample ranged from 12 to 47 GPa. In one additional experiment, the fused silica sample was backed by a LiF window and a double-shock state reaching 63 GPa was produced by reshock from 46 to 63 GPa at the LiF window. The experimental parameters are provided in the Supplemental Material, Table S1 [35]. Laser interferometry was used to measure impact velocities and the continuum stress, and density states were determined by impedance matching using the known equations of state of fused silica and LiF. *In situ* x-ray diffraction measurements were obtained using a single bunch ( $\sim 100$  ps) of the APS storage ring operated in 24-bunch mode. For each experiment, four x-ray diffraction images each separated by 153.4 ns were recorded. Experiments were designed such that one or two x-ray diffraction frames were obtained while the shock wave propagated through the fused silica but before it reached the rear surface. The x-ray diffraction data for the frames corresponding to the most fully compressed material were analyzed in detail to determine the structure and state of the shock-compressed material. See the Supplemental Material for further details [35].

Figure 1 shows a series of azimuthally integrated diffraction patterns obtained during uniform stress states ranging from 17 to 63 GPa. The diffraction patterns correspond to frames captured during the uniform shock state prior to the shock front having traversed the entire thickness of the sample. Owing to the transmission geometry of the experiments (Supplemental Material, Fig. S4 [35]), the measurements sample some amount of uncompressed  $\text{SiO}_2$  and/or elastically compressed material. The fraction of uncompressed material was less than 8% for all patterns shown in Fig. 1 except for the pattern at 23 GPa, in which 22% of the  $\text{SiO}_2$  remained uncompressed. An additional shot collected at 12 GPa is not shown in Fig. 1, as the fraction of uncompressed material was nearly 40%. The elastic precursor is overdriven at peak stresses above 25 GPa. Note also that the incident x-ray beam passes through the body of the polycarbonate projectile giving rise to additional amorphous scattering at low angle (Supplemental Material, Figs. S6 and S9 [35]).

At 34 GPa and below, no crystalline diffraction peaks from the sample were detected, but diffuse scattering features were observed at two-theta values less than  $15^\circ$ , indicating that fused silica remained amorphous

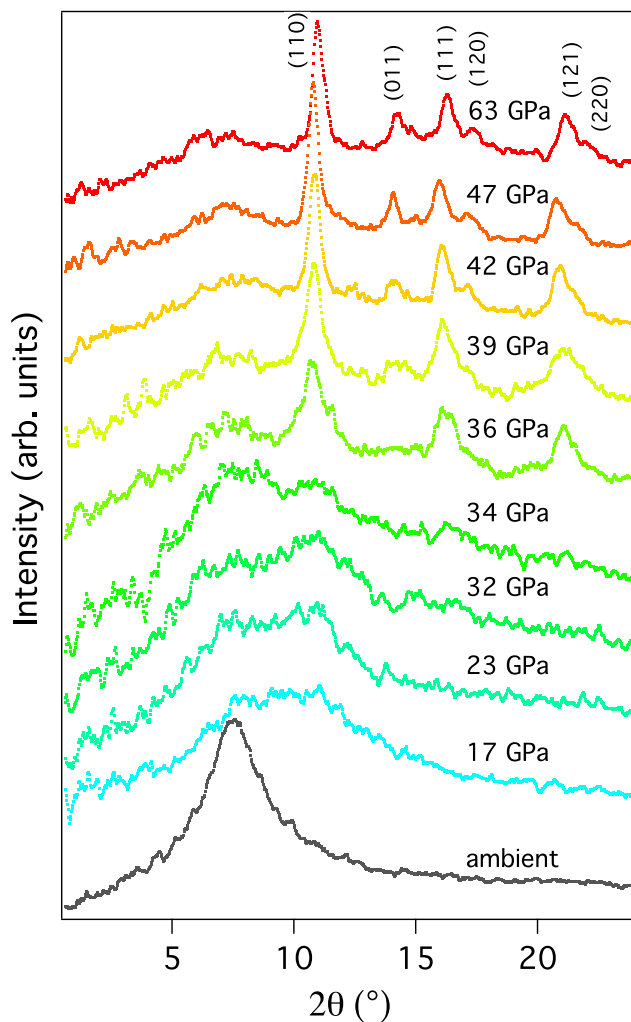


FIG. 1. Azimuthally integrated x-ray diffraction data collected for a series of plate-impact experiments with peak stress states between 17 and 63 GPa. Stishovite peaks are labeled with  $hkl$  values.

when shock compressed to these conditions (Fig. 1 and Supplemental Material, Fig. S9 [35]). At stresses of 36 GPa and above, we observe sharp diffraction peaks demonstrating that fused silica transformed to a crystalline phase (Fig. 1 and Supplemental Material, Fig. S5 [35]). The diffraction rings are relatively smooth, indicating that the high-pressure phase does not have significant texture.

When compressed under static pressure,  $\text{SiO}_2$  adopts a series of crystalline phases from quartz to coesite ( $C2/c$ ) to stishovite (rutile structure,  $P4_2/mnm$ ) to the  $\text{CaCl}_2$ -type phase ( $Pnmm$ ) [48]. In addition, a number of metastable forms of  $\text{SiO}_2$  have been observed experimentally or predicted theoretically [49]. To identify the phase crystallizing on the fused silica Hugoniot, we performed diffraction simulations that account for the shape of the pink x-ray beam (Supplemental Material, S3 [35]). Figure 2 shows excellent agreement between the background-subtracted

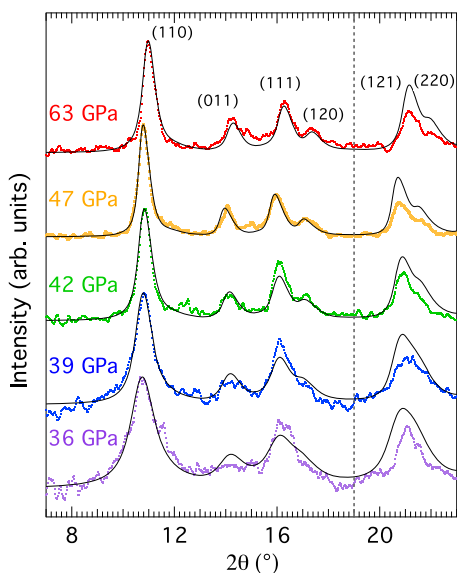


FIG. 2. X-ray diffraction data in the high-pressure region. The fits (black curves) overlay experimental data (points). Least-squares fits were performed to determine the lattice parameters and peak widths for stishovite diffraction peaks. The vertical dotted line denotes the extent of the fit region, above which detector-sensitivity effects render intensity data quantitatively unreliable.

data and diffraction simulations using the rutile structure, demonstrating that fused silica transforms to stishovite upon shock compression above 34 GPa. Within the resolution of our measurements, there is no evidence for any peak splitting or enhanced broadening of the stishovite (120) and (121) peaks that would indicate a further transformation to a  $\text{CaCl}_2$ -type phase. Other possible high-pressure phases including coesite,  $\alpha$ - $\text{PbO}_2$ -type, and  $\text{Fe}_2\text{N}$ -type [26,27,49] are not consistent with the observed diffraction data.

Our results allow us to explain previously ambiguous features of the behavior of fused silica under shock compression. Notably, the abrupt change in compressibility along the Hugoniot at 35 GPa corresponds precisely to where we identify the amorphous-crystalline phase change (Fig. 3). This is also consistent with *in situ* electrical conductivity measurements of fused silica [14] that reported a discontinuous decrease in resistivity at 35 GPa. More generally, our results show the viability of amorphous to crystalline phase transformations within the  $\sim 100$ -ns time scale of plate-impact experiments.

Figure 3 shows that the crystal densities determined from x-ray diffraction above 34 GPa are consistent with previous continuum Hugoniot data. This figure includes a calculated Hugoniot for stishovite using a Mie-Grüneisen equation of state (Supplemental Material, S5 [35]), demonstrating that our x-ray diffraction results are consistent with the expected properties of stishovite along the Hugoniot. The thermodynamic parameters used for the calculated Hugoniot

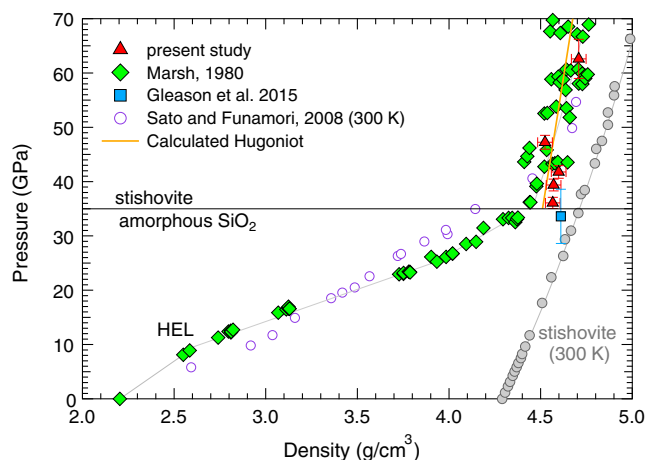


FIG. 3. Shock Hugoniot curve for fused silica. Red triangles show x-ray densities from this study. Continuum Hugoniot data from gun experiments [50] are shown as green diamonds along with the x-ray density (blue square) determined from laser-driven compression [25]. Also shown are 300-K static compression data for stishovite (gray circles) [51] and fused silica (open purple circles) [52]. HEL (Hugoniot elastic limit).

curve in Fig. 3 are listed in the Supplemental Material, Table S3 [35].

Our results are also consistent with recent molecular dynamics simulations which report the conversion of fused silica to polycrystalline stishovite on time scales of a few nanoseconds at pressures above 50 GPa [53]. The transformation is described by a homogeneous nucleation and growth model involving only small-scale atomic motions with atomic neighbor memories largely erased in the transformation. The grain sizes inferred from our results are consistent with extrapolations of the molecular dynamics simulations from  $\sim 1$  ns to hundreds of nanoseconds, as described below.

We observe pronounced sharpening of the diffraction peaks between 36 and 47 GPa (Fig. 2). This is particularly evident for the strong stishovite (110) peak. This suggests that grain growth is enhanced as the temperature rises with increasing shock pressure. The degree of peak broadening was determined by convolving Lorentzian profiles with the diffraction simulations. Sample broadening was assessed after accounting for broadening from the x-ray source, instrumental broadening, and broadening due to finite sample thickness (Supplemental Material, S3.4 [35]). We attribute this broadening to grain size by applying the Scherrer equation to the full width at half maximum of the stishovite (110) peak using [54]

$$\langle d \rangle = \frac{0.94\lambda}{\beta \cos(\theta)}. \quad (1)$$

Here,  $\langle d \rangle$  is the mean stishovite grain size,  $\lambda = 0.539 \text{ \AA}$  is the x-ray wavelength,  $\beta$  is the peak width, and  $\theta$  is the

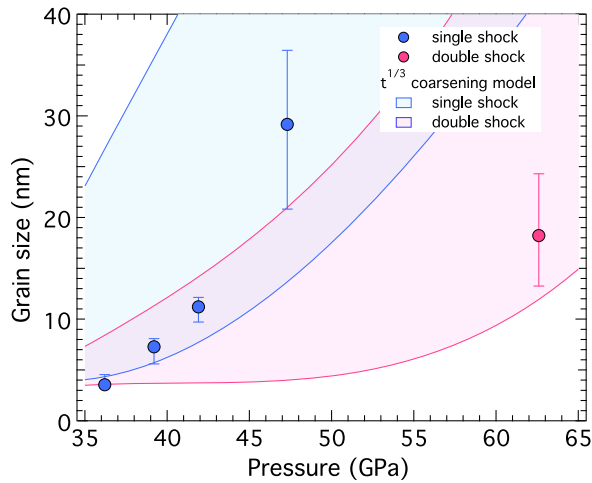


FIG. 4. Grain sizes determined using the Scherrer equation from the current experiments (circles) along with range of grain sizes predicted using the  $t^{1/3}$  coarsening law from molecular dynamics [53] for both single-shock (blue field) and double-shock (pink field) states. The large uncertainties in grain size calculations arise primarily from uncertainty in the shock temperature.

Bragg angle. This equation provides a lower limit on the grain size of the transformed material in the shocked state. Figure 4 shows our results together with calculated grain sizes from molecular dynamics simulations of stishovite formed from shock-compressed fused silica [53].

In the simulations, thermal energy promotes the rapid nucleation of nanocrystals from local regions of coherent short-range order. This is followed by a grain coalescence phase where grain growth depends primarily on the shock temperature. When shock compressed into the high-pressure region, fused silica first adopts a dense disordered structure. This intermediate structure is transient and within picoseconds local regions of order nucleate, and transformation to a fine grained stishovite occurs in a matter of nanoseconds. The subsequent rate of grain growth is given by [53]

$$\langle d \rangle = (\langle d_0 \rangle^3 + K \Delta t)^{1/3}, \quad (2)$$

$$K = K_0 \exp\left(\frac{-Q}{k_B T}\right). \quad (3)$$

Here,  $\langle d \rangle$  is the average grain size in nm,  $\langle d_0 \rangle$  is the grain size at the start of the grain coalescence growth phase,  $\Delta t$  is the time after start of coalesce,  $k_B$  is Boltzmann's constant, and  $T$  is the temperature.  $\Delta t$  was taken as the diffraction frame time relative to impact. The values for  $K_0$ ,  $Q$ , and  $\langle d_0 \rangle$  are given in Ref. [53].

The uncertainty in our result arises primarily from uncertainty in the shock temperature. Calculated single-shock temperatures range from 3200 to  $5800 \pm 500$  K between 36 and 63 GPa. Double-shock temperatures in this range are  $2400\text{--}4300 \pm 500$  K (Supplemental Material,

S5 [35]). Figure 4 shows that the grain sizes determined from our experiments at time scales of hundreds of nanoseconds are consistent with the model inferred from molecular dynamics simulations up to 1.5 ns.

Our results demonstrate that the region of the Hugoniot from 10 to 35 GPa is not a mixed-phase region but instead corresponds to densification of the starting glass (Figs. 1 and 3). Under room-temperature compression,  $\text{SiO}_2$  glass initially undergoes rearrangement of  $\text{SiO}_4$  tetrahedra followed by a continuous change in coordination with increasing pressure, transforming to a dense, nearly octahedrally coordinated structure by about 35 GPa [52,55]. We envision a similar process occurring in the shock-compressed glass. The amorphous structure seen in Fig. 1 consists of two broad components, one at low angle which is insensitive to pressure and a second at higher angle that moves to higher two-theta values with compression. Below 35 GPa, this second amorphous feature is peaked at  $Q \sim 2.2 \text{ \AA}^{-1}$  [ $Q = (4\pi/\lambda) \sin \theta$ ], consistent with the first strong diffraction peak of  $\text{SiO}_2$  glass observed in static compression experiments in this pressure range [52,55–57]. The low-angle feature seen in all shots at  $2\theta \sim 7^\circ$  is a combined result of scattering from the polycarbonate projectile along with scattering from any remaining uncompressed (or elastically compressed)  $\text{SiO}_2$ .

A comparison of static compression with continuum Hugoniot data shows that the density of glass at 300 K is generally similar to Hugoniot densities up to 35 GPa (Fig. 3). In fact, from 20 to 35 GPa, the density of the glass along the Hugoniot exceeds that under 300-K compression, despite the higher temperature of the Hugoniot states. This suggests that high-temperature compression allows for additional compression mechanisms, enabling the glass to achieve a denser state than it can at lower temperatures. This is consistent with static compression data for fused silica, which show enhanced densification upon compression at high temperatures [58,59].

Based on analogy with static compression, recovery experiments, and theoretical models, we infer that the shock-compressed glass at 34 GPa is a nearly six-coordinated glass with a high degree of “stishovitelike” short-range order [52,60,61]. This disordered phase may be similar to the intermediate structure seen at early times in molecular dynamics simulations [53]. Our calculated shock temperature at this pressure ( $\sim 3100 \pm 500$  K) is broadly consistent with previous shock temperature measurements on fused silica [6,62,63]. Above this temperature threshold, the requisite thermal energy is available to overcome an activation barrier, promoting the small atomic displacements required to transform the highly coordinated glass into crystalline stishovite on shock-compression time scales. This type of transformation arises from local correlated motions of atoms as opposed to longer length scale diffusive rearrangements, allowing for the transformation to proceed to completion over short time scales.

Our results are in marked contrast to recent laser-compression experiments that reported evidence for the formation of stishovite from fused silica at pressures below 35 GPa on nanosecond time scales [25,64]. While the highest pressure datum in that study ( $34 \pm 5$  GPa) overlaps our results, stishovite peaks were also observed at 19 GPa and below where we observe only amorphous material despite 2 orders of magnitude longer compression time. In the experiments of Refs. [25,64], pressures were estimated only indirectly from measurements of the transit time through the entire sample package. The reported pressures may be significantly underestimated (see Ref. [25] Supplementary Material, p. 9). Laser shock experiments may suffer from stress nonuniformity and nonsteadiness of the shock wave. In contrast, plate-impact experiments produce well-defined planar waves and steady states of compression. The stress states in our sample are well constrained by the precisely measured impact velocities and the known equations of state of fused silica and lithium fluoride. The consistency of our results with Hugoniot and other continuum data also provides strong support for our measurements.

Our study resolves the long controversy about the nature of the fused silica Hugoniot. Upon shock compression above the elastic limit up to 34 GPa, stishovite adopts a dense amorphous structure, comparable to its behavior under static compression. At shock pressures above 34 GPa, fused silica transforms to polycrystalline stishovite, consistent with the sharp change in the compressibility of the Hugoniot curve at this pressure. Stishovite grain sizes inferred from diffraction peak widths are consistent with the extrapolation of results from molecular dynamics simulations which identify a homogenous nucleation and two-stage grain growth model for the formation of stishovite under shock compression. Our results demonstrate that the region between 9 and 35 GPa represents a densification region rather than a true mixed-phase region, across which the glass evolves from a four- to six-coordinated structure. It is only above 34 GPa that there is the requisite thermal energy to drive crystallization.

We thank Paulo Rigg and the staff of Dynamic Compression Sector for assistance with impact experiments. Binyamin Glam (Soreq, Nuclear Research Center) provided experimental assistance. Yogendra Gupta is thanked for discussions and a reading of the manuscript. This research was supported by the Defense Threat Reduction Agency Grant No. HDTRA1-15-1-0048. Washington State University provided experimental support through the U.S. Department of Energy National Nuclear Security Agency Award No. DE-NA0002007. This work is based upon experiments performed at the Dynamic Compression Sector, which is operated by Washington State University under Department of Energy/National Nuclear Security Agency Award No. DE-NA0002442. This research used the resources of

the Advanced Photon Source, a Department of Energy Office of Science User Facility operated for the Department of Energy Office of Science by Argonne National Laboratory under Contract No. DE-AC02-06CH11357.

\*sjtracy@princeton.edu

- [1] R. G. McQueen, S. P. Marsh, and J. N. Fritz, *J. Geophys. Res.* **72**, 4999 (1967).
- [2] J. A. Akins and T. J. Ahrens, *Geophys. Res. Lett.* **29**, 31-1 (2002).
- [3] Y. Zhang, T. Sekine, H. He, Y. Yu, F. Liu, and M. Zhang, *Geophys. Res. Lett.* **41**, 4554 (2014).
- [4] J. L. Mosenfelder, P. D. Asimow, D. J. Frost, D. C. Rubie, and T. J. Ahrens, *J. Geophys. Res. Solid Earth* **114**, B01203 (2009).
- [5] J. M. Brown and R. G. McQueen, *J. Geophys. Res. Solid Earth* **91**, 7485 (1986).
- [6] G. A. Lyzenga, T. J. Ahrens, and A. C. Mitchell, *J. Geophys. Res. Solid Earth* **88**, 2431 (1983).
- [7] J. H. Nguyen and N. C. Holmes, *Nature (London)* **427**, 339 (2004).
- [8] Q. Williams, R. Jeanloz, J. Bass, B. Svendsen, and T. J. Ahrens, *Science* **236**, 181 (1987).
- [9] J. A. Akins, S.-N. Luo, P. D. Asimow, and T. J. Ahrens, *Geophys. Res. Lett.* **31**, L14612 (2004).
- [10] H. Huang, Y. Fei, L. Cai, F. Jing, X. Hu, H. Xie, L. Zhang, and Z. Gong, *Nature (London)* **479**, 513 (2011).
- [11] T. S. Duffy and T. J. Ahrens, *J. Geophys. Res. Solid Earth* **100**, 529 (1995).
- [12] C. W. Thomas and P. D. Asimow, *J. Geophys. Res. Solid Earth* **118**, 5738 (2013).
- [13] S.-N. Luo, J. L. Mosenfelder, P. D. Asimow, and T. J. Ahrens, *Geophys. Res. Lett.* **29**, 36-1 (2002).
- [14] K. Kondo, A. Sawaoka, and T. J. Ahrens, *J. Appl. Phys.* **52**, 5084 (1981).
- [15] F. Barmes, L. Souillard, and M. Mareschal, *Phys. Rev. B* **73**, 224108 (2006).
- [16] A. Salleo, S. T. Taylor, M. C. Martin, W. R. Panero, R. Jeanloz, T. Sands, and F. Y. Genin, *Nat. Mater.* **2**, 796 (2003).
- [17] L. Hallo, A. Bourgeade, C. Mezel, G. Travaillle, D. Hebert, B. Chimier, G. Schurtz, and V. T. Tikhonchuk, *Appl. Phys. A* **92**, 837 (2008).
- [18] M. Grujcic, J. S. Snipes, and S. Ramaswami, *J. Mater. Eng. Perform.* **25**, 995 (2016).
- [19] C. S. Alexander, L. C. Chhabildas, W. D. Reinhart, and D. W. Templeton, *Int. J. Impact Eng.* **35**, 1376 (2008).
- [20] S.-N. Luo, T. J. Ahrens, and P. D. Asimow, *J. Geophys. Res. Solid Earth* **108**, 2421 (2003).
- [21] S. L. Chaplot and S. K. Sikka, *Phys. Rev. B* **61**, 11205 (2000).
- [22] H. Tan and T. J. Ahrens, *J. Appl. Phys.* **67**, 217 (1990).
- [23] J. C. Boettger, *J. Appl. Phys.* **72**, 5500 (1992).
- [24] R. G. McQueen, J. N. Fritz, and S. P. Marsh, *J. Geophys. Res.* **68**, 2319 (1963).
- [25] A. E. Gleason, C. A. Bolme, H. J. Lee, B. Nagler, E. Galtier, D. Milathianaki, J. Hawreliak, R. G. Kraus, J. H. Eggert,

- D. E. Fratanduono, G. W. Collins, R. Sandberg, W. Yang, and W. L. Mao, *Nat. Commun.* **6**, 8191 (2015).
- [26] T. Sekine, M. Akaishi, and N. Setaka, *Geochim. Cosmochim. Acta* **51**, 379 (1987).
- [27] L. C. Chhabildas and D. E. Grady, in *Shock Waves in Condensed Matter, 1983*, edited by J. R. Asay, R. A. Graham, and G. K. Struab (Elsevier, New York, 1984), pp. 175–178.
- [28] W. R. Panero, L. R. Benedetti, and R. Jeanloz, *J. Geophys. Res. Solid Earth* **108**, 2015 (2003).
- [29] F. Langenhorst, *Earth Planet. Sci. Lett.* **128**, 683 (1994).
- [30] F. Langenhorst and A. Deutsch, *Elements* **8**, 31 (2012).
- [31] T. G. Sharp and P. S. DeCarli, in *Meteorites and the Early Solar System II*, edited by D. S. Lauretta and H. Y. McSween (University of Arizona Press, Tucson, AZ, 2015), pp. 653–677.
- [32] A. J. Gratz, W. J. Nellis, J. M. Christie, W. Brocious, J. Swegle, and P. Cordier, *Phys. Chem. Miner.* **19**, 267 (1992).
- [33] N. M. Kuznetsov, in *High-Pressure Shock Compression of Solids VII.*, edited by V. E. Fortov, L. V. Alt’shuler, R. F. Trunin, and A. I. Funtikov (Springer, New York, 2015), pp. 275–295.
- [34] P. Berterretche, T. de Ressaquier, M. Hallouin, and J. P. Petitot, *J. Appl. Phys.* **96**, 4233 (2004).
- [35] See Supplemental Material at <http://link.aps.org/supplemental/10.1103/PhysRevLett.120.135702> for details concerning experimental procedure, data reduction, and analysis, which includes Refs. [36–47].
- [36] L. M. Barker and R. E. Hollenbach, *J. Appl. Phys.* **43**, 4669 (1972).
- [37] O. T. Strand, D. R. Goosman, C. Martinez, T. L. Whitworth, and W. W. Kuhlow, *Rev. Sci. Instrum.* **77**, 083108 (2006).
- [38] T. J. Ahrens, in *Geophysics, Methods in Experimental Physics*, edited by G. H. Sammis and T. L. Henyey (Academic Press, New York, 1987), Vol. 24, pp. 185–235.
- [39] Q. Liu, X. Zhou, X. Zeng, and S.-N. Luo, *J. Appl. Phys.* **117**, 045901 (2015).
- [40] T. Sun and K. Fezzaa, *J. Synchrotron Radiat.* **23**, 1046 (2016).
- [41] A. P. Hammersley, S. O. Svensson, M. Hanfland, A. N. Fitch, and D. Hausermann, *High Press. Res.* **14**, 235 (1996).
- [42] R. G. McQueen, S. P. Marsh, J. W. Taylor, J. N. Fritz, and W. J. Carter, in *High Velocity Impact Phenomena*, edited by R. Kinslow (Academic Press, New York, 1970), pp. 294–417.
- [43] F. Jiang, G. D. Gwanmesia, T. I. Dyuzheva, and T. S. Duffy, *Phys. Earth Planet. Inter.* **172**, 235 (2009).
- [44] R. A. Robie and D. R. Waldbaum, in *Geological Survey Bulletin 1259* (U.S. Government Printing Office, Washington, DC, 1968).
- [45] G. F. Davies, *J. Geophys. Res.* **77**, 4920 (1972).
- [46] J. R. Smyth and T. C. McCormick, in *Mineral Physics and Crystallography: A Handbook of Physical Constants*, edited by T. J. Ahrens (American Geophysical Union, Washington, DC, 1995), pp. 1–17.
- [47] Y. Sumino and O. L. Anderson, in *Handbook of Physical Properties of Rocks, 1984*, edited by R. S. Carmichael (CRC Press, Boca Raton, FL, 1984), Vol. 3, p. 94.
- [48] R. J. Hemley, C. T. Prewitt, and K. J. Kingma, *Rev. Mineral. Geochem.* **29**, 41 (1994).
- [49] L. S. Dubrovinsky, N. A. Dubrovinskaia, V. Prakapenka, F. Seifert, F. Langenhorst, V. Dmitriev, H.-P. Weber, and T. L. Bihan, *Phys. Earth Planet. Inter.* **143–144**, 231 (2004).
- [50] S. P. Marsh, *LASL Shock Hugoniot Data* (University of California Press, Los Angeles, 1980).
- [51] D. Andrault, R. J. Angel, J. L. Mosenfelder, and T. Le Bihan, *Am. Mineral.* **88**, 301 (2003).
- [52] T. Sato and N. Funamori, *Phys. Rev. Lett.* **101**, 255502 (2008).
- [53] Y. Shen, S. B. Jester, T. Qi, and E. J. Reed, *Nat. Mater.* **15**, 60 (2016).
- [54] B. D. Cullity, *Elements of X-Ray Diffraction* (Addison-Wesley, Reading, MA, 1956), p. 381.
- [55] C. J. Benmore, E. Soignard, S. A. Amin, M. Guthrie, S. D. Shastri, P. L. Lee, and J. L. Yarger, *Phys. Rev. B* **81**, 054105 (2010).
- [56] C. Prescher, V. B. Prakapenka, J. Stefanski, S. Jahn, L. B. Skinner, and Y. Wang, *Proc. Natl. Acad. Sci. U.S.A.* **114**, 10041 (2017).
- [57] Y. Inamura, Y. Katayama, W. Utsumi, and K. I. Funakoshi, *Phys. Rev. Lett.* **93**, 015501 (2004).
- [58] F. S. Elkin, V. V. Brazhkin, L. G. Khvostantsev, O. B. Tsiok, and A. G. Lyapin, *J. Exp. Theor. Phys. Lett.* **75**, 342 (2002).
- [59] M. Guerette, M. R. Ackerson, J. Thomas, F. Yuan, E. B. Watson, D. Walker, and L. Huang, *Sci. Rep.* **5**, 15343 (2015).
- [60] E. M. Stolper and T. J. Ahrens, *Geophys. Res. Lett.* **14**, 1231 (1987).
- [61] O. Tschauer, S. N. Luo, P. D. Asimow, T. J. Ahrens, D. C. Swift, T. E. Tierney, D. L. Paisley, and S. J. Chipera, *High Press. Res.* **24**, 471 (2004).
- [62] M. Millot, N. Dubrovinskaia, A. Cernok, S. Blaha, L. Dubrovinsky, D. G. Braun, P. M. Celliers, G. W. Collins, J. H. Eggert, and R. Jeanloz, *Science* **347**, 418 (2015).
- [63] H. Sugiura, K. Kondo, and A. Sawaoka, *J. Appl. Phys.* **53**, 4512 (1982).
- [64] A. E. Gleason, C. A. Bolme, H. J. Lee, B. Nagler, E. Galtier, R. G. Kraus, R. Sandberg, W. Yang, F. Langenhorst, and W. L. Mao, *Nat. Commun.* **8**, 1481 (2017).